crystals

MDPI

Article

Mid-Infrared Dual-Wavelength Passively Q-Switched Er: SrF_2 Laser by $CsPbCl_3$ Quantum Dots Absorber

Leilei Guo [1,2], Maorong Wang [1,2,*], Yifan Zhang [1,2], Shuaiyi Zhang [1,2], Kai Zhong [3], Qiuling Zhao [1,2], Lihua Teng [1,2], Xia Wang [1,2,*] and Jianquan Yao [3]

1 College of Mathematics and Physics, Qingdao University of Science and Technology, Qingdao 266061, China
2 Shandong Advanced Optoelectronic Materials and Technologies Engineering Laboratory, Qingdao 266061, China
3 Key Laboratory of Optoelectronics Information Technology, Ministry of Education, School of Precision Instrument and Opto-Electronics Engineering, Tianjin University, Tianjin 300072, China
* Correspondence: qust@vip.126.com (M.W.); phwangxia@163.com (X.W.)

Abstract: A passively Q-switched compact dual-wavelength Er: SrF_2 laser, operating at a 2729.73 nm and 2747.2 nm wavelength, was demonstrated by utilizing $CsPbCl_3$ quantum dots (QDs) as a saturable absorber (SA). The maximum average output power with the shortest duration of 510 ns and a repetition rate of 45 kHz was achieved at 190 mW, and the corresponding maximum single pulse energy and the peak power were 73.69 μJ and 141.7 W, respectively. The results present an efficient dual-wavelength laser source, and the halogen perovskite quantum dot has the potential to be employed as an excellent saturable absorber in mid-infrared pulsed solid-state lasers.

Keywords: Q-switched; solid-state; $CsPbCl_3$ quantum dots; pulsed laser

Citation: Guo, L.; Wang, M.; Zhang, Y.; Zhang, S.; Zhong, K.; Zhao, Q.; Teng, L.; Wang, X.; Yao, J. Mid-Infrared Dual-Wavelength Passively Q-Switched Er: SrF_2 Laser by $CsPbCl_3$ Quantum Dots Absorber. *Crystals* **2022**, *12*, 1265. https://doi.org/10.3390/cryst12091265

Academic Editors: Julien Brault and Alessandra Toncelli

Received: 3 August 2022
Accepted: 4 September 2022
Published: 6 September 2022

1. Introduction

In the mid-infrared (MIR) region, pulsed laser sources around 3 μm are regularly employed in various applications, including laser surgery, gas sensing, environmental monitoring, nonlinear spectroscopy science, and so on [1–3], even for the generation of terahertz using the difference frequency method (DFG) based on various dual-wavelength pulsed lasers operating from nano-second to pico-second [4–7]. In the MIR region, rare-earth ions, Tm^{3+}, Er^{3+}, and Ho^{3+} [8–10], are usually used for laser crystal doping emitting at ~2.8–3 μm. Because of the much longer lifetime of $^4I_{13/2}$ compared with $^4I_{11/2}$ of Er^{3+} [11], a self-terminating process will affect the high-efficiency output of the laser. However, this situation can be improved by increasing the doping concentration.

Up to now, there have been reports of continuous-wave and pulsed laser operation in Er:SrF_2 crystals [12,13]. In 2018, Liu et al. substantiated Er^{3+}-doped SrF_2 crystal growth using the temperature gradient technique, and they subsequently demonstrated a passive Q-switched mode-locked laser using a semiconductor mirror and bismuth nanosheets as a saturable absorber [14]. The results confirmed that an SrF_2 crystal with a low phonon energy of ~280 cm^{-1} is suitable for producing mid-infrared lasers owing to the more negligible probability of nonradioactive transitions [12]. Simultaneously, schemes for generating pulsed lasers include Q-switched, Q-switched mode-locked, and continuous mode-locked. Active pulsed lasers with electro-optic (EO) modulation or acousto-optic (AO) modulation [15–18] can obtain narrower pulse widths, but the system volume will be larger and more complex, which is not convenient for compactness and miniaturization. Relatively speaking, although the pulse width obtained with passive modulation will be wider, this method is more conducive to integrating systems, such as miniaturized terahertz radiation sources. By adopting an appropriate saturable absorber (SA) as a passive modulator, Q-switched and mode-locked operations are not difficult to achieve. Innumerable SAs have been reported, such as doped crystals of U^{4+}: SrF_2 and Cr^{3+}:

YAG [19,20] with better stability and performance, and novel micro–nano materials with more compact cavities have also been reported. Among these SAs, two-dimensional micro–nano materials have attracted much more attention because of their superior nonlinear absorption characteristics over a wide wavelength range, including graphene [21,22], black phosphorus (BP) [23], perovskite-structured materials [24–26], hexagonal boron nitride (hBN) [27], transition-metal dichalcogenides (TMDs) [28], and so on, resulting from the arrow band gap or direct band gap, high carrier mobility, and fast switching speed [29–32].

In comparison, benzylamine lead (II) bromide and all-inorganic perovskites have attracted extensive attention due to their better room temperature stability and absorption wavelength tunability for visible-to-infrared light based on their perovskite structure and quantum confinement effects [33]. In 2019, the nonlinear optical properties of benzylamine lead (II) bromide perovskites were verified by Aamir Mushtaq et al., and they demonstrated the tunable nonlinear behaviors from a saturable absorber (SA) to reverse saturable absorption (RSA), which is attributed to the interplay between single- and two-photon absorption by the carriers in the conduction band [34]. In 2021, Xu et al. reported the nonlinear optical characteristics of all-inorganic $CsPbBr_3$ perovskite quantum dot-doped borosilicate glasses [35]. Benefits from the high gain of the fiber itself, passively Q-switched or mode-locked in a fiber laser by all-inorganic halide perovskite ($CsPbBr_3$) and organic–inorganic halide perovskite quantum dots ($CH_3NH_3PbI_3$, $CH_3NH_3PbI_{3-x}Cl_x$, $MASnI_3$) can be seen in public reports [36,37]. However, the resulting pulse width is still not as good as active modulation. Particularly, as with all solid-state lasers, typical pulse widths generated using Q-switched perovskite are around ~660 ns [38,39], which could be better improved by designing the cavity and optimizing the saturable absorber.

In this paper, we prepared high-quality, all-inorganic perovskite $CsPbCl_3$ quantum dots, stable at room temperature, using a hotplate synthesis method. Simultaneously, the nonlinear absorption properties of $CsPbCl_3$ quantum dots were verified using an 80 MHz femtosecond laser, confirming that it can be used as a saturable absorber. Then, we created a passively Q-switched compact dual-wavelength Er: SrF_2 laser by utilizing the $CsPbCl_3$ quantum dots as an SA operating stabilizer.

2. Device Characterization and Experiment

High-quality $CsPbCl_3$ QDs were prepared with a hotplate synthetic scheme adding Cs-oleate into $PbCl_2$ precursor stock solution in gas-free conditions at 150 °C [40]. The original reaction solution dispersed in hexane was centrifuged at 8000 rpm for 10 min in a high-speed centrifuge, and then we took the washed supernatant for characterization.

The average size and morphology of the $CsPbCl_3$ QDs were characterized by transmission electron microscopy (TEM, HT7800, Hitachi, Tokyo, Japan). The TEM image of $CsPbCl_3$ QDs depicted a shape close to cubic, and the average size was 6~8 nm. As can be seen in Figure 1a, the $CsPbCl_3$ QDs were distributed equally without overlapping, which indicated an excellent mono-dispersing in a non-polar solvent. The photoluminescence (PL) spectrum exhibited in Figure 1b was recorded with our self-built micro-measuring system equipped with a spectrometer (USB4000, Ocean Optics, FL, USA), and the wavelength of the pump laser source was 360 nm. The center wavelength of the PL emission peak was 408.9 nm, and the half-peak width (FWHM) was 15.8 nm, which represents good agreement with Ref. [40].

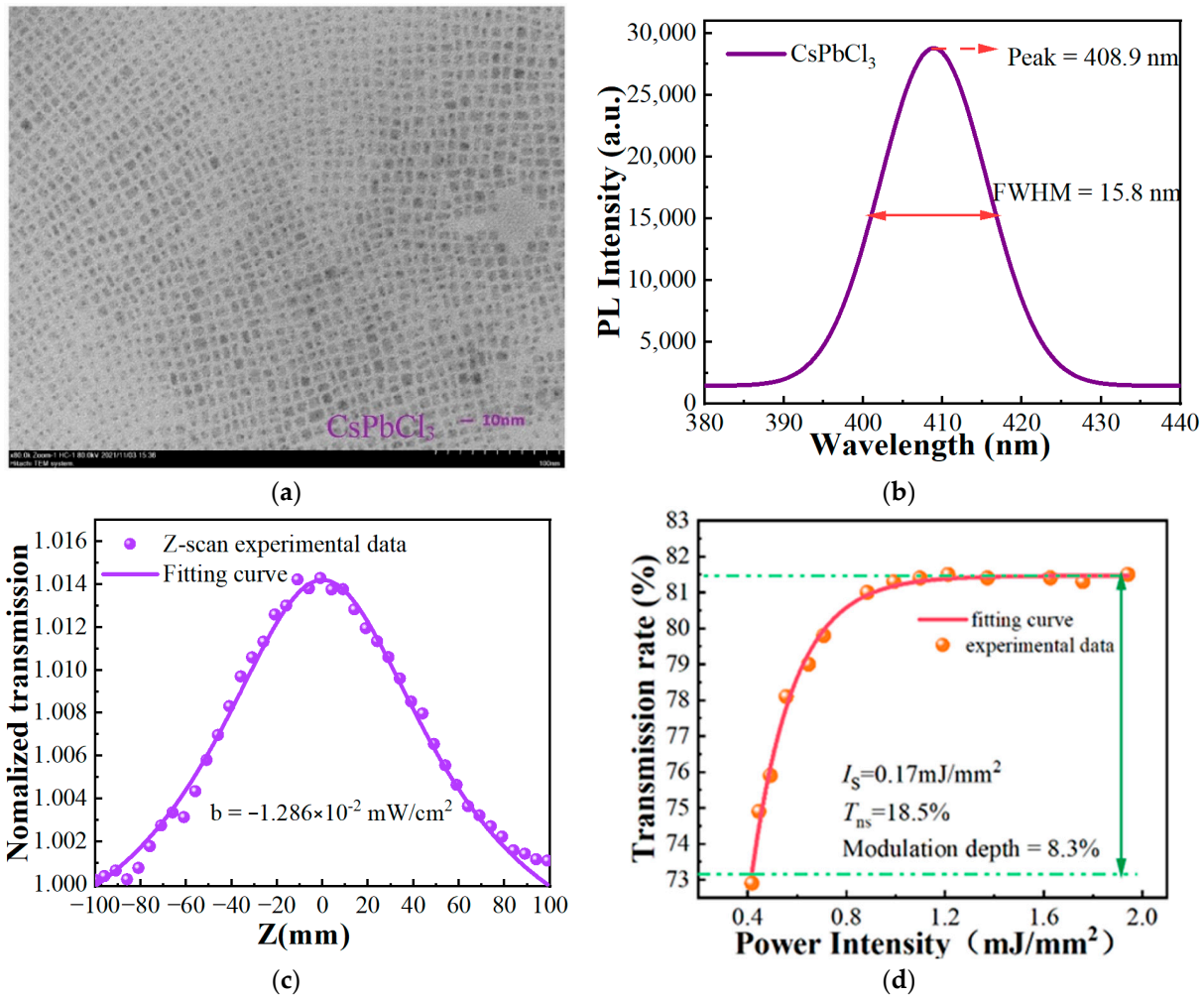

Figure 1. (**a**) TEM image of the $CsPbCl_3$ perovskite QDs; (**b**) normalized PL spectra for the $CsPbCl_3$ perovskite QDs' dispersion; (**c**) normalized open-aperture Z-scan results for $CsPbCl_3$ QDs at 500 mW incident laser energy with an 80 MHz repetition and an 808 nm femtosecond laser; (**d**) nonlinear transmission of $CsPbCl_3$ QDs with a modulation depth of 8.3% and 0.17 mJ/mm^2 saturation intensity (the green lines represent the upper and lower limits of the modulation depth).

The nonlinear absorption characteristic of the QDs was measured using an open-aperture (OA) Z-scan system with an 80 MHz repetition rate femtosecond laser and a pulse width of 60 fs at 800 nm. In the Z-scan experiment, the laser beam was focused by a 200 mm lens and collimated by a 200 mm lens to fill the aperture of the objective lens. The Z-scan experimental results (represented by dots) and the theoretical fitting (represented by lines) in Formula (1) [41] for the nonlinear absorption are shown in Figure 1c, and they exhibited saturable absorption properties.

$$T = (z, S = 1) = \sum_{m=0}^{\infty} \frac{[-q_0(z)]^m}{(m+1)^{3/2}} \quad (1)$$

where $q_0(z) = bI_0L_{eff}/(1 + z^2/z_0^2)$, I_0 is the on-axis peak intensity, b is the nonlinear absorption coefficient, z is the location of the sample, $z_0 = (\pi\omega_0\hat{}2)/\lambda$ expresses the Rayleigh range, ω_0 is the waist radius of the beam, $L_{eff} = (1 - e\hat{}(L\alpha_0))/\alpha_0$ is the effective length, L is the sample length, and α_0 is the linear absorption coefficient. The nonlinear absorption coefficient of the $CsPbCl_3$ QDs was approximately 1.28×10^{-2} mW/cm^2.

The nonlinear transmission of $CsPbCl_3$ QDs was measured by the 3-μm pulsed laser, shown in Figure 1d. Curve fitting for the extracted data was exhibited using Formula (2) [42]:

$$T = 1 - \Delta R \cdot \exp(-I/I_s) - T_{ns} \quad (2)$$

where T is the transmission of the QDs-SA, I_s the saturable intensity, ΔR is the modulation depth, and T_{ns} is the unsaturated loss. The saturable intensity, modulation depth, and unsaturated loss for the $CsPbCl_3$ QDs-SA obtained by fitting the measured data using Formula (2) were 0.17 mJ/mm^2, 8.3%, and 18.5%, respectively.

Subsequently, the passively Q-switched dual-wavelength solid-state laser based on the $CsPbCl_3$ perovskite QD saturable absorber was investigated. The passively Q-switched laser experimental diagram is presented in Figure 2. To ensure that the SA was placed inside the laser cavity with high efficiency, we needed to fabricate a laser cavity mirror with high transmittance covered by a $CsPbCl_3$ QDs dispersion. The $CsPbCl_3$ QD saturable absorber was prepared by way of spin-coating. Firstly, we added 4 mL n-hexane to the prepared $CsPbCl_3$ QDs, which were placed in a 4 mL centrifuge tube. Then, the centrifuge tube was put into an ultrasonic cleaner to dissolve the $CsPbCl_3$ QDs fully for 30 min. The tube was centrifuged at 8000 rpm for 10 min to remove larger crystal particles. Finally, the supernatant, including the $CsPbCl_3$ QDs, was collected, which was dropped on the YAG mirror operating at 2000 rpm in a spin coater. Then, the mirror was placed in a dry box for 10 min, creating the $CsPbCl_3$ QDs-SA.

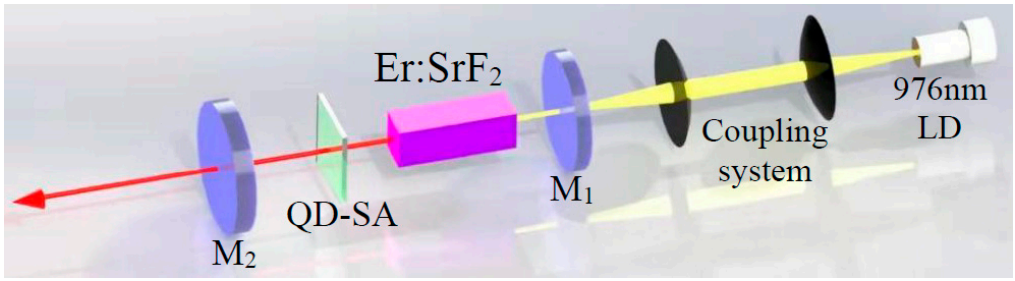

Figure 2. Passively Q-switched experimental setup with the $CsPbCl_3$ QDs-SA.

The pump source (BWT, Beijing, China) was a fiber-coupled semiconductor laser with a central wavelength of 976 nm. The fiber core diameter of the laser was 105 μm. Through a 1:1 coupling system with a focal length of 46.6 mm, a numerical aperture of 0.22, and light transmittance from 808 to 1064 nm, the pump laser was focused on the laser crystal. The laser gain medium was a 4 at. % Er: SrF_2 crystal with a size of $3 \times 3 \times 10$ mm^3. In the experiment, the crystal was wrapped in indium foil, mounted in a copper heat sink, and cooled at a water-cooled temperature of 16 °C. A familiar straight compact cavity of about 8 cm in length was used as a laser cavity, and the mirror, M_1, worked as an input flat mirror with high transmittance (HT) at 976 nm and high reflectivity (HR) at 2940 nm. Another mirror, M_2, was a planoconcave output mirror with different curvature radiuses: a 100 mm curvature radius with two transmittances of 1% and 4% (T = 1% or 4%, R = −100 mm) and a 200 mm curvature radius with 1% transmittance (T = 1%, R = −200 mm). The output pulsed laser was recorded by a detector (PPS03, Vigo, Mazowiecki, Poland) and an oscilloscope (DSO-X3104A, Agilent Technologies, CA, USA). The laser spectrum and the power were detected with a spectrometer (OSA207C, Thorlabs, NJ, USA) and a power meter (PM100D, Thorlabs, NJ, USA).

3. Results and Discussion

The output performance between the continuous wave (CW) laser power and the passively Q-Switched laser power versus the absorption pump power is described in Figure 3a,b, respectively. The CW output power was first measured with three output mirrors. When the transmittance and curvature radius of M_2 were 1% and 100 mm, a

maximum output power of 210 mW was achieved with an absorbed pump power of 2.87 W, corresponding to an optical-to-optical conversion efficiency of 7.3% and a slope efficiency of 7.35%. For the output mirror with values of T = 4% and R = −100 mm, the CW output power reached the maximum value of 105 mW, and for the output mirror with T = 1% and R = −200 mm, the CW output power reached the maximum value of 190 mW. Then, the $CsPbCl_3$ QDs-SA was inserted into the laser cavity, as shown in the laser setup in Figure 2. The Q-switched laser pulse started appearing when the absorbed pump power approached 0.51 W. The average output power is shown in Figure 3b, and the maximum Q-switched output powers were 75 mW, 67 mW, and 77 mW with M_2: T = 4%, R = −100 mm, and T = 1%, R = −100 mm or −200 mm, respectively. The corresponding highest optical conversion efficiency and slope efficiency were 2.68% and 2.97%, respectively. Illustrations in Figure 3a,b present the diversification of the laser emission spectrum recorded with an optical spectrometer, which clearly shows that the central wavelengths were from 2729.73 nm and 2747.19 nm in the CW laser mode to 2728.24 nm and 2745.97 nm in the Q-switched laser mode. The change in the laser wavelength caused by the nonlinear phase delay resulting from the high optical intensity of the continuous light output in the pulsed light output is consistent with Refs. [43,44].

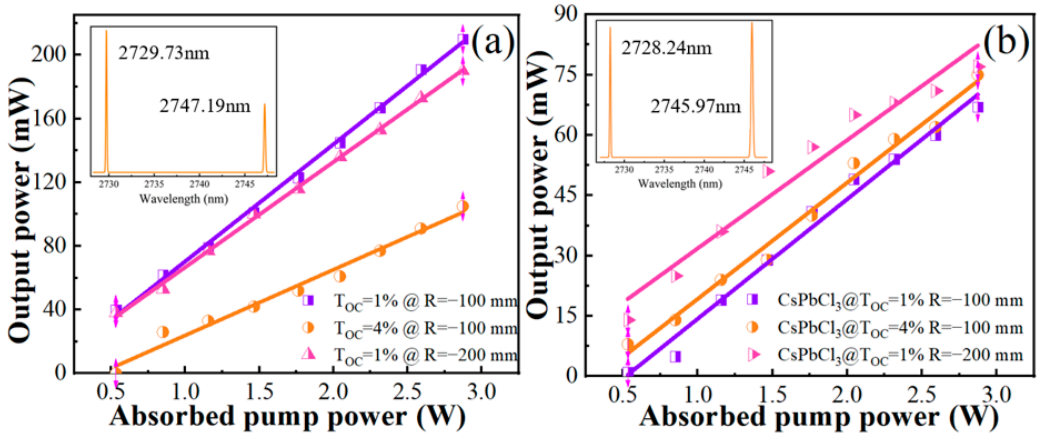

Figure 3. (**a**) Average output power of CW laser; (**b**) average output power of Q-switched laser. Insert laser emission spectrum.

After adding the QDs-SA to the laser cavity, the pulse duration, repetition rate, single pulse energy, and peak power of the Q-switched operation were drawn as functions of the absorbed pump power, as seen in Figure 4. It can be seen that the repetition rate gradually increased and the pulse width gradually became narrower as the absorbed pump power rose. When the parameters of M_2 were T = 1% and R = −100 mm, the maximum repetition frequency was 39 kHz, and the narrowest pulse width was 520 ns. Replaced by T = 4%, the narrowest pulse of 510 ns was gained with a maximum repetition frequency of 45 kHz. In the case where the output mirror with values of T = 1% and R = −200 mm was used, the maximum repetition frequency was 43 kHz, and the narrowest pulse width was 800 ns. Compared with the $CsPbBr_3$ and $CH_3NH_3PbI_3$ perovskite SAs reported in Ref [38,39], the minimum pulse duration was 510 ns at a repetition rate of 45 kHz. Our pulse duration was better than theirs. In the case of M2, with the values of T = 1% and R = −100 mm, the maximum single pulse energy was 73.69 μJ, and the corresponding peak power was 141.7 W.

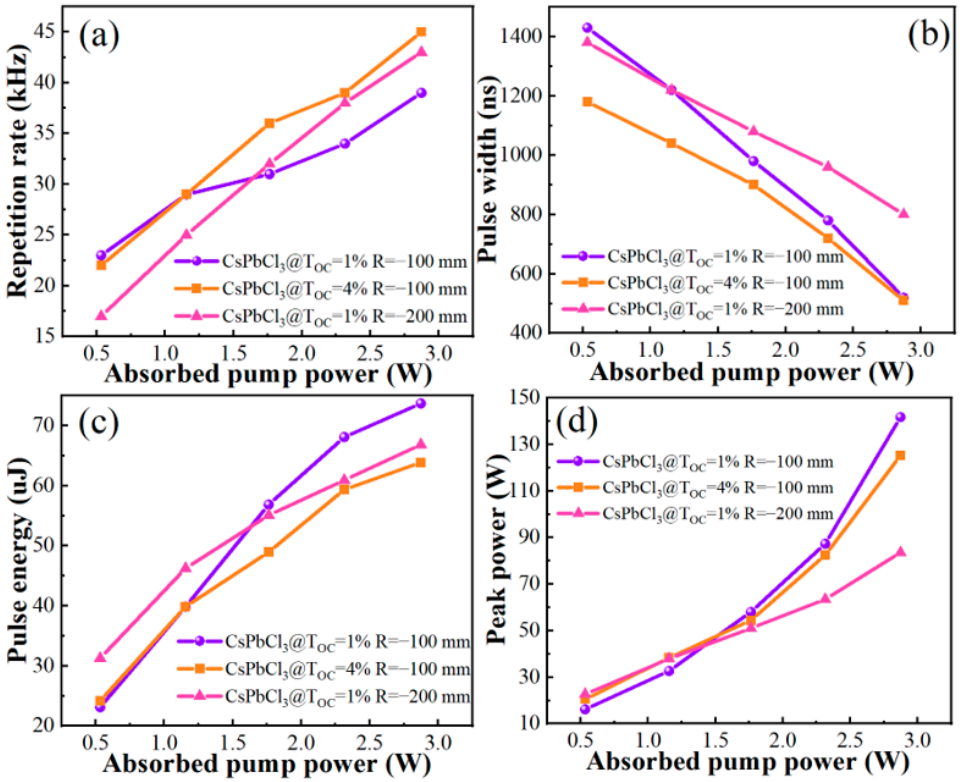

Figure 4. (**a**) Repetition rate and (**b**) pulse width versus absorbed pump power for the passively Q-switched laser; (**c**) Pulse energy and (**d**) peak power versus absorbed pump power for the Q-switched laser.

With the absorbed pump power increasing, the repetition rate increased, while the pulse duration decreased gradually. Typical Q-switched pulse trains are shown in Figure 5, depicting the pulse sequence of a single pulse under the output mirror with different transmittances. The minimum pulse duration was 510 ns at a repetition rate of 45 kHz.

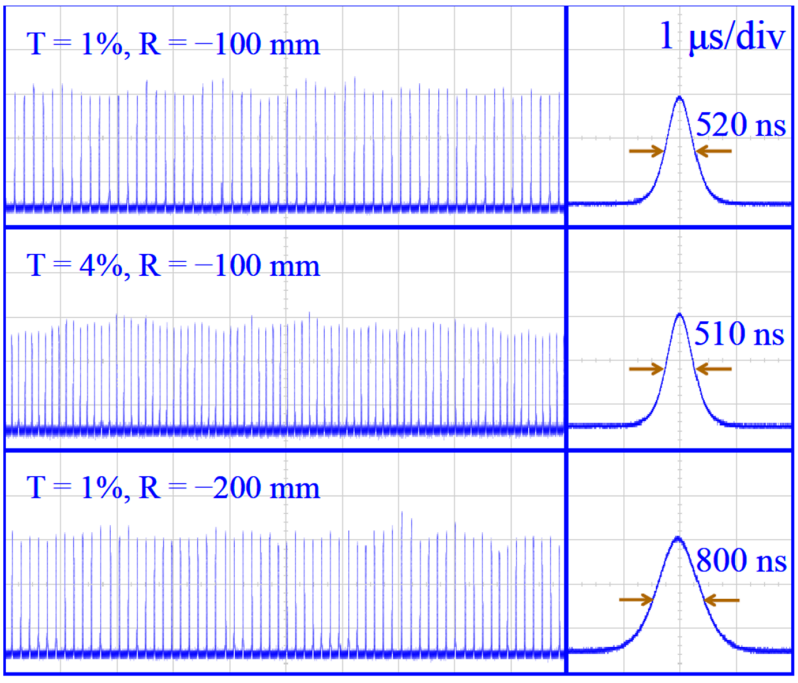

Figure 5. Typical pulse trains and temporal pulse profiles displayed by the oscilloscope.

4. Conclusions

In conclusion, we demonstrated a 2729.73 nm and 2747.19 nm passively Q-switched compact dual-wavelength solid-state Er: SrF_2 laser with a $CsPbCl_3$ QDs-SA. The maximum average output power with the shortest duration of 510 ns and a repetition rate of 45 kHz was measured at 190 mW, and the corresponding maximum single pulse energy and peak power were 73.69 μJ and 141.7 W respectively. The results present an efficient dual-wavelength laser source, and the $CsPbCl_3$ QDs-SA shows potential for mid-infrared pulsed laser modulation.

Author Contributions: Data curation, Y.Z. and Q.Z.; formal analysis, S.Z. and J.Y.; investigation, K.Z. and L.T.; project administration, X.W.; supervision, M.W.; writing—original draft, L.G. All authors have read and agreed to the published version of the manuscript.

Funding: This research was funded by the National Natural Science Foundation of China (Grant No. 61905127, Grant No. 12174212, and Grant No. 11874232) and the Open Fund of the Key Laboratory of Optoelectronic Information Technology Education (Tianjin University) (Grant No. 2022KFKT015).

Institutional Review Board Statement: Not applicable.

Informed Consent Statement: Not applicable.

Data Availability Statement: Not applicable.

Acknowledgments: Thanks to the editor for the technical support.

Conflicts of Interest: The authors declare no conflict of interest.

References

1. Walsh, J.T.; Flotte, T.J.; Deutsch, T.F. Er: YAG laser ablation of tissue: Effect of pulse duration and tissue type on thermal damage. *Lasers Surg. Med.* **1989**, *9*, 314–326. [CrossRef] [PubMed]
2. Hugi, A.; Villares, G.; Blaser, S.; Liu, H.C.; Faist, J. Mid-infrared frequency comb based on a quantum cascade laser. *Nature* **2012**, *492*, 229–233. [CrossRef] [PubMed]
3. Antipov, S.; Hudson, D.D.; Fuerbach, A.; Jackson, S.D. High-power mid-infrared femtosecond fiber laser in the water vapor transmission window. *Optica* **2016**, *3*, 1373–1376. [CrossRef]
4. Schaar, J.E.; Vodopyanov, K.L.; Fejer, M.M. Intracavity terahertz-wave generation in a synchronously pumped optical parametric oscillator using quasi-phase-matched GaAs. *Opt. Lett.* **2007**, *32*, 1284–1286. [CrossRef]
5. Schellr, M.; Yarborough, J.M.; Moloncy, J.V.; Fallahi, M.; Koch, M.; Koch, S.W. Room temperature continuous wave milliwatt terahertz source. *Opt. Express* **2010**, *18*, 27112–27117. [CrossRef]
6. Kiessling, J.; Breunig, I.; Schunemann, P.G.; Buse, K.; Vodopyanov, K.L. High power and spectral purity continuous-wave photonic THz source tunable from 1 to 4.5 THz for nonlinear molecular spectroscopy. *New J. Phys.* **2013**, *15*, 105014–105025. [CrossRef]
7. Creeden, D.; McCarthy, J.C.; Ketteridge, P.A.; Southward, T.; Schunemann, P.G.; Komiak, J.J.; Dove, W.; Chicklis, E.P. Compact Fiber-Pumped Terahertz Source Based on Difference Frequency Mixing in ZGP. *IEEE J. Sel. Top. Quantum Electron.* **2007**, *13*, 732–737. [CrossRef]
8. Wang, Y.X.; Liu, W.X.; Zhang, Z.H.; Strzep, A.; Liu, J.; Chen, Z.Q.; Ma, F.K.; Su, L.B. Laser-diode-pumped Tm:SrF_2 single crystal for high efficiency CW laser operation at ~2 μm. *Opt. Lett.* **2022**, *47*, 1117–1120. [CrossRef]
9. Guan, X.; Zhan, L.; Zhu, Z.; Xu, B.; Xu, H.; Cai, Z.; Cai, W.; Xu, X.; Zhang, J.; Xu, J. Continuous-wave and chemical vapor deposition graphene-based passively Q-switched Er:Y_2O_3 ceramic lasers at 2.7 μm. *Appl. Opt.* **2018**, *57*, 371. [CrossRef]
10. Li, C.; Liu, J.; Jiang, S.; Xu, S.; Ma, W.; Wang, J.; Xu, X.; Su, L. 2.8 μm passively Q-switched Er: CaF_2 diode-pumped laser. *Opt. Mater. Express* **2016**, *6*, 1570. [CrossRef]
11. Fang, Z.; Sun, D.; Luo, J.; Zhang, H.; Zhao, X.; Quan, C.; Hu, L.; Cheng, M.; Zhang, Q.; Yin, S. Thermal analysis and laser performance of a GYSGG/Cr, Er, Pr: GYSGG composite laser crystal operated at 2.79 μm. *Opt. Express* **2017**, *25*, 21349–21357. [CrossRef] [PubMed]
12. Ma, W.; Qian, X.; Wang, J.; Liu, J.; Fan, X.; Liu, J.; Su, L.; Xu, J. Highly efficient dual-wavelength mid-infrared CW Laser in diode end-pumped Er: SrF_2 single crystals. *Sci. Rep.* **2016**, *6*, 36635. [CrossRef] [PubMed]
13. Liu., J.; Liu, J.; Yang, J.; Ma, W.; Wu, Q.; Su, L. Efficient mid-infrared laser under different excitation pump wavelengths. *Opt. Lett.* **2017**, *42*, 3908–3911. [CrossRef] [PubMed]
14. Liu, J.; Feng, X.; Fan, X.; Zhang, Z.; Zhang, B.; Liu, J.; Su, L. Efficient continuous-wave and passive Q-switched mode-locked Er3+: CaF_2-SrF_2 lasers in the mid-infrared region. *Opt. Lett.* **2018**, *43*, 2418–2421. [CrossRef]
15. Nie, H.; Shi, B.; Xia, H.; Hu, J.; Zhang, B.; Yang, K.; He, J. High-repetition-rate kHz electro-optically Q-switched Ho, Pr: YLF 2.9 μm bulk laser. *Opt. Express* **2018**, *26*, 33671–33677. [CrossRef]

16. Wang, L.; Wang, J.; Yang, J.; Wu, X.; Sun, D.; Yin, S.; Jiang, H.; Wang, J.; Xu, C. 2.79 μm high peak power LGS electro-optically Q-switched Cr, Er: YSGG laser. *Opt. Lett.* **2013**, *38*, 2150–2152. [CrossRef]
17. Pushkin, A.V.; Mazur, M.M.; Sirotkin, A.A.; Firsov, V.V.; Potemkin, F.V. Powerful 3μm lasers acousto-optically Q-switched with KYW and KGW crystals. *Opt. Lett.* **2019**, *44*, 4837–4840. [CrossRef]
18. Duan, X.; Chen, G.; Shen, Y.; Zheng, L.; Su, L. High-Power Cotinuous-Wave and Acousto-Optical Q-Switched Ho:$(Sc_{0.5}Y_{0.5})_2SiO_5$ Laser Pumped by Laser Diode. *Chin. Phys. Lett.* **2019**, *36*, 064201. [CrossRef]
19. Liu, J.; Zong, M.; Wang, D.; Zhang, Z.; Su, L. Acousto-optic Q-switched Er:CaF_2-SrF_2 laser at 2.73 μm. *Infrared Phys. Technol.* **2021**, *116*, 103758. [CrossRef]
20. Liu, J.; Fan, M.; Su, L.; Jiang, D.; Ma, F.; Zhang, Q.; Xu, J. Laser performance of diode-pumped Nd, Y-codoped CaF_2-SrF_2 mixed crystal. *Laser Phys.* **2014**, *24*, 035802. [CrossRef]
21. Novoselov, K.S.; Geim, A.K.; Morozov, S.V.; Jiang, D.; Zhang, Y.; Dubonos, S.V.; Grigorieva, I.V.; Firsov, A.A. Electric Field Effect in Atomically Thin Carbon Films. *Science* **2004**, *306*, 666–669. [CrossRef] [PubMed]
22. Zhang, H.; Bao, Q.; Tang, D.; Zhao, L.; Loh, K. Large energy soliton erbrium-doped fiber laser with a graphene-polymer composite mode locker. *Appl. Phys. Lett.* **2009**, *95*, 141103. [CrossRef]
23. Li, L.; Yu, Y.; Ye, G.J.; Ge, Q.; Ou, X.; Wu, H.; Feng, D.; Chen, X.; Zhang, Y. Black phosphorus field-effect transistors. *Nat. Nanotechnol.* **2014**, *9*, 372–377. [CrossRef] [PubMed]
24. Huang, B.; Yi, J.; Jiang, G.; Miao, L.; Hu, W.; Zhao, C.; Wen, S. Passively Q-switched vectorial fiber laser modulated by hybrid organic-inorganic perovskites. *Opt. Mater. Express* **2017**, *7*, 1220–1227. [CrossRef]
25. Bao, X.; Mu, H.; Chen, Y.; Li, P.; Li, L.; Li, J.; Khan, Q.; Zhang, Y.; Zhang, H.; Bao, Q. Ytterbium-doped fiber laser passively mode locked by evanescent field interaction with $CH_3NH_3SnI_3$ perovskite saturable absorber. *J. Phys. D Appl. Phys.* **2018**, *51*, 375106. [CrossRef]
26. Li, P.; Yao, C.; Yang, T.; Wang, Z.; Lin, H.; Xu, Y.; Li, L.; Mu, H.; Shivananju, B.N.; Zhang, Y.; et al. Two-Dimensional $CH_3NH_3PbI_3$ Perovskite Nanosheets for Ultrafast Pulsed Fiber Lasers. *ACS Appl. Mater. Inter.* **2017**, *9*, 12759–12765. [CrossRef]
27. Kim, K.K.; Hsu, A.; Jia, X.; Kim, S.M.; Shi, Y.; Hofmann, M.; Nezich, D.; Rodriguez-Nieva, J.F.; Dresselhaus, M.; Palacios, T.; et al. Synthesis of monolayer hexagonal boron nitride on Cu foil using chemical vapor deposition. *Nano Lett.* **2012**, *12*, 161–166. [CrossRef]
28. Liu, H.; Luo, A.; Wang, F.; Tang, R.; Liu, M.; Luo, Z.C.; Xu, W.; Zhao, C.; Zhang, H. Femtosecond pulse erbium-doped fiber laser by a few-layer MoS_2 saturable absorber. *Opt. Lett.* **2014**, *39*, 4591–4594. [CrossRef]
29. Low, T.; Roldán, R.; Wang, H.; Xia, F.; Avouris, P.; Moreno, L.M.; Guinea, F. Plasmons and screening in monolayer and multilayer black phosphorus. *Phys. Rev. Lett.* **2014**, *113*, 106802. [CrossRef]
30. Kocnig, S.P.; Doganov, R.A.; Schmidt, H.; Castro Ncto, A.H.; OEzyilmaz, B. Electric field effect in ultrathin black phosphorus. *Appl. Phys. Lett.* **2014**, *104*, 103106.
31. Xia, F.; Wang, H.; Jia, Y. Rediscovering black phosphorus as an anisotropic 2D material for optoelectronics and electronics. *Nat. Commun.* **2014**, *5*, 4458. [CrossRef] [PubMed]
32. Ma, J.; Lu, S.; Guo, Z.; Xu, X.; Zhang, H.; Tang, D.; Fan, D. Few-layer black phosphorus based saturable absorber mirror for pulsed solid-state lasers. *Opt. Express* **2015**, *23*, 22613–22618. [CrossRef]
33. Yan, Z.; Hu, Z.; Yue, L.; Xu, J.; Tang, X.; Tang, Y. CsPbBr3 nanocrystal saturable absorber for mode-locking ytterbium fiber laser. *Appl. Phys. Lett.* **2016**, *108*, 831.
34. Mushtaq, A.; Kushavah, D.; Ghosh, S.; Pal, S.K. Nonlinear optical properties of benzylamine lead(II) bromide perovskite microdisks in femtosecond regime. *Appl. Phys. Lett.* **2019**, *114*, 051902. [CrossRef]
35. Xu, Z.; Chen, T.; Zhang, D.; Zheng, G.; Wu, J.; Yan, J.; Liu, X.; Qiu., J. Linear and nonlinear optical characteristics of $CsPbBr_3$ perovskite quantum dots-doped borosilicate glasses. *J. Eur. Ceram. Soc.* **2021**, *41*, 729–734. [CrossRef]
36. Liu, B.; Guo, L.; Chen, W.W.; Tang, X.S.; Gao, C.; Cao, Y.L.; Li, Y.J.; Zhu, T. 1.6 μm dissipative soliton fiber laser mode-locked by cesium lead halide perovskite quantum dots. *Opt. Express* **2018**, *26*, 7155–7162. [CrossRef]
37. Jiang, G.; Miao, L.; Yi, J.; Huang, B.; Peng, W.; Zou, Y.; Huang, H.; Hu, W.; Zhao, C.; Wen, S. Ultrafast pulse generation from erbium-doped fiber laser modulated by hybrid organic-inorganic halide perovskites. *Appl. Phys. Lett.* **2017**, *110*, 161111. [CrossRef]
38. Li, J.; Dong, H.; Xu, B.; Zhang, S.; Cao, Z.; Wang, J.; Zhang, L. CsPbBr3 perovskite quantum dots: Saturable absorption properties and passively Q-switched visible lasers. *Photonics Res.* **2017**, *5*, 457–460. [CrossRef]
39. Zhang, R.; Fan, J.; Zhang, X.; Yu, H.; Zhang, H.; Mai, Y.; Xu, T.; Wang, J.; Snaith, H.J. Nonlinear Optical Response of Organic-Inorganic Halide Perovskites. *ACS Photonics* **2016**, *3*, 371–377. [CrossRef]
40. Otero-Martínez, C.; García-Lojo, D.; Pastoriza-Santos, I.; Pérez-Juste, J.; Polavarapu, L. Dimensionality Control of Inorganic and Hybrid Perovskite Nanocrystals by Reaction Temperature: From No-Confinement to 3D and 1D Quantum Confinement. *Angew. Chem. Int. Ed. Engl.* **2021**, *60*, 26677–26684. [CrossRef]
41. Sheik-Bahae, M.; Said, A.A. Sensitive measurement of optical nonlinearities using a single beam. *IEEE J. Quantum Electron.* **1990**, *26*, 760–769. [CrossRef]
42. Lin, M.; Peng, Q.; Hou, W.; Fan, X.; Liu, J. 1.3 μm Q-switched solid-state laser based on few-layer ReS_2 saturable absorber. *Opt. Laser Technol.* **2019**, *109*, 90–93. [CrossRef]

43. Liu, J.; Liu, J.; Guo, Z.; Zhang, H.; Ma, W.; Wang, J.; Su, L. Dual-wavelength Q-switched Er: SrF_2 laser with a black phosphorus absorber in the mid-infrared region. *Opt. Express* **2016**, *24*, 30289. [CrossRef] [PubMed]
44. Kong, L.C.; Xie, G.Q.; Yuan, P.; Qian, L.J.; Wang, S.X.; Yu, H.H.; Zhang, H.J. Passive Q-Switching and Q-Switched Mode-Locking Operations of 2 μm Tm: CLNGG Laser with MoS_2 Saturable Absorber Mirror. *Photonics Res.* **2015**, *3*, A47–A50. [CrossRef]